Research Article

Lubomír Lapčík*, Martin Vašina, Barbora Lapčíková, David Hui, Eva Otyepková, Richard W. Greenwood, Kristian E. Waters, and Jakub Vlček

Materials characterization of advanced fillers for composites engineering applications

Abstract: Four different minerals were investigated; hollow spheres of calcium carbonate, platy mica, needle like wollastonite and glassy perlite and characterized via iGC for surface energy, Freeman powder rheology for flow characterization, cyclic uniaxial die compaction for modulus of elasticity and frequency dependent sound absorption properties. Particle surface energy and particle shape strongly affected the packing density of powder beds. In the case of higher porosity and thus lower bulk density, the powders acoustic absorption was higher in comparison with higher packing density materials. Surface energy profiles and surface energy distributions revealed clear convergence with powder rheology data, where the character of the powder flow at defined consolidation stresses was mirroring either the high cohesion powders properties connected with the high surface energy or powder free flowing characteristics, as reflected in low cohesion of the powder matrix.

Keywords: mineral fillers, surface properties, sound absorption, mechanical properties, powder rheology

1 Introduction

Modern globalized automotive and aerospace production companies apply advanced composites and coating systems in their final product lines. At the present time, the goal is to enhance overall price/performance ratio and increase productivity with respect to the processing time, using a lean technology approach and energy input [1]. That is why a wide range of synthetic or natural based micro/nano fillers were being used in technical practice [2–4]. For that reason detailed knowledge of the filler particles surface interface is important for exact adjustments of the consecutive technological operations during production cycles. Micro/nano particles filled synthetic polymers are commonly used for the structural as well as non-structural components and advanced coatings applications [5]. Previously minerals served as the additives in polymer systems mainly as a cost reducing component [6]. Progressing technological improvements in minerals processing and polymer chemistry allowed their novel role as the functional additives, thus bringing specific mechanical and functional properties to the final composites structures [5, 7–9]. The packing density of the powder bed is strongly dependent on the applied consolidation stress, surface energy [10], surface roughness and particle shape of the individual particles [11–13]. That is why our focus in this study was aimed at the characterization of the physico-chemical (surface energy, surface energy distribution and surface energy profiles characterization) and material properties (powder rheology, sound absorption and die compaction

*Corresponding Author: Lubomır Lapčık: Regional Centre of Advanced Technologies and Materials, Department of Physical Chemistry, Faculty of Science, Palacky University, 17. Listopadu 12, 771 46 Olomouc, Czech Republic; Tomas Bata University in Zlin, Faculty of Technology, Nam. T.G. Masaryka 275, 760 01 Zlin, Czech Republic; Email: lapcikl@seznam.cz
Martin Vašina: Tomas Bata University in Zlin, Faculty of Technology, Nam. T.G. Masaryka 275, 760 01 Zlin, Czech Republic; VŠB-Technical University of Ostrava, Department of Hydromechanics and Hydraulic Equipment, Faculty of Mechanical Engineering, 17. Listopadu 15/2172, 708 33 Ostrava-Poruba, Czech Republic
Barbora Lapčıková: Regional Centre of Advanced Technologies and Materials, Department of Physical Chemistry, Faculty of Science, Palacky University, 17. Listopadu 12, 771 46 Olomouc, Czech Republic; Tomas Bata University in Zlin, Faculty of Technology, Nam. T.G. Masaryka 275, 760 01 Zlin, Czech Republic
David Hui: University of New Orleans, Composite Materials Research Laboratory, 2000 Lakeshore Dr., New Orleans, LA 70148, United States of America

Eva Otyepková, Jakub Vlček: Regional Centre of Advanced Technologies and Materials, Department of Physical Chemistry, Faculty of Science, Palacky University, 17. Listopadu 12, 771 46 Olomouc, Czech Republic
Richard W. Greenwood: School of Chemical Engineering, University of Birmingham, Edgbaston, Birmingham, B15 2TT, United Kingdom of Great Britain and Northern Ireland
Kristian E. Waters: Department of Mining and Materials Engineering, McGill University, M.H. Wong Building, 3610 University Street, Montreal, H3A 0C5, Québec, Canada

Table 1: Studied mineral samples labelling and description

Sample	Description
1	Calcium carbonate hollow spheres (University of Birmingham, UK), d_{50} = 991 nm diameter[*], density 2.40 g/cm^{3}[#].
2	Muscovite Mica (Imerys, Kings Mountains, USA), d_{50} = 17 μm diameter[*], specific surface area 9.7 m^2/g, platy with an aspect ratio 1.7, density 0.45 g/cm^{3}[#].
3	Wollastonite type VANSIL W-10 (Vanderbilt Minerals, Norwalk, USA), d_{50} = 49 μm diameter[*], specific surface area 0.5 m^2/g, needle like with an aspect ratio 13.5, density 0.65 g/cm^{3}[#].
4	Perlite, volcanic glass (Supreme Perlite Company, USA), d_{50} = 447 nm diameter[*], density 1.10 g/cm^{3}[#].

[*]As measured in Palacky University lab. [#]According to manufacturer's data sheet.

behavior) both in the individual as well as in particles collective cooperation setups of free poured powder beds and die compression configurations. During die compression the deformation of the free powder bed is continuously proceeding, hence increasing the compression stress in the system. This is recorded as the stress-displacement dependency as obtained for given deformation rates and applied maximum stress. Obtained loading and unloading curves reflect the intimate inter-particle interactions and ongoing processes of deformation and displacement associated with the proceeding applied compression stress. The following sequence of individual processes during agglomeration has been recognized; namely the feed of loose packing, elastic–plastic contact deformation, pore filling by fine particles, plastic deformation of particles to create large contact areas, breakage of edges, particle breakage and plastic deformation of entire sample [14]. During the loading cycle, the deformation took place in contacts as well as the volume deformation of individual powder particles [15, 16], reflecting compaction of the sample with translation and rotation movements of particles, at relatively small contact deformations followed by the deformation of entire particles and their breakage [14]. Elastic recovery of the compacted powder bed is an important processing parameter affecting consecutive creation of defects and fractures in the compressed material due to the proceeding fast recovery or spring back, thus influencing final mechanical properties of the compressed body [14, 17].

2 Materials

As filler particles the inorganic minerals calcium carbonate hollow spheres (The University of Birmingham), muscovite mica (Imerys, Kings Mountains, USA), wollastonite type VANSIL W-10 (Vanderbilt Minerals, Norwalk, USA) and perlite (Supreme Perlite Company, USA) were used in

this study. The basic description, labelling and physical parameters of the studied fillers are given in Table 1.

3 Methods

3.1 Thermal analysis

For powder moisture content thermogravimetry (TG) and differential thermal analysis (DTA) experiments were performed on a simultaneous DTA-TG apparatus (Shimadzu DTG 60, Japan). Measurements were performed at a heat flow rate of 10°C/min in a static air atmosphere at the temperature range from 30°C to 300°C. Samples moisture content as determined by thermal analysis (TG DTG) ranged from 0.1 to 0.9 wt.%.

3.2 Inverse gas chromatography surface energy analysis

Inverse gas chromatography (iGC) was performed by surface energy analyzer (SEA) (Surface Measurement Systems, UK). Samples were placed in 4 mm (internal diameter) columns to give a total surface area of approximately 0.5 m^2. Nonane, octane, hexane, heptane, dichloromethane, acetone, acetonitrile, ethyl acetate and ethanol were used as eluents for iGC. All reagents were obtained from Sigma Aldrich (USA) and were of analytical grade. The injection of vapors was controlled in order to give pre-determined fractional coverage of the sample. By gradually increasing the amount of vapors injected, it is possible to build up a surface heterogeneity plot [5, 18]. Surface energy distribution was calculated according to the standard methodology as described by Mohammadi-Jam and Waters [19].

3.3 Powder rheology

Powder rheology measurements were conducted on a FT4 Powder rheometer (Freeman Technology, UK). All experiments were performed under the ambient laboratory temperature of 24°C and relative humidity of 45%. Consolidation stresses of 9 kPa were used for samples 1, 2 and 4, but 22 kPa for sample 3.

3.4 Uniaxial die compression testing

Uniaxial die compression testing was performed on universal testing machine Autograph AGS-X (Shimadzu, Japan) equipped with the Compact Thermostatic Chamber TCE Series. A stainless steel cylindrical die of 13 mm inner diameter and 40 mm height was used. Measurements were performed at 0.2, 1.2 and 10 mm/min deformation rates. Each measurement was repeated three times and mean average values were calculated. The compressive as well as release stress-strain dependencies were then determined. From these tests the modulus of elasticity (E) was calculated as the slope of the first linear part of unloading curve (down ramp), and the bulk modulus (K) was calculated from the same data according to Eg. (1), where at this phase of unloading only the elastic response of the studied powder material took place [14, 20]:

$$K_{ab} = \frac{\sigma_z^A - \sigma_z^B}{\epsilon_z^A - \epsilon_z^B} = K + 4K\frac{1 - 2\nu}{1 + 2\nu} \quad (1)$$

where K_{ab} is the slope of the down ramp from maximum axial stress (point A) to half the maximum axial stress (point B), σ_z is the axial stress, ϵ_z is the axial strain and ν is the Poisson's ratio [20]. In this investigation, the Poisson's ratio was assumed to have a value of 0.25 as referred earlier by [20, 21].

3.5 Powder bed sound absorption testing

Sound absorption coefficient measurements of freely poured powder beds were performed by means of the transfer function method ISO 10534-2 standard [22]. There were measured frequency dependencies of the sound absorption coefficient by means of a two-microphone impedance tube (BK 4206) in combination with three-channel signal PULSE multi-analyzer (BK 3560-B-030) and power amplifier (BK 2706) in the frequency range of 150-6400 Hz (Brüel & Kjær, Denmark). The normal incidence sound wave absorption of the tested loose powder samples of defined layer thickness (ranging from 10 to 100 mm) was

determined. All experiments were performed under ambient laboratory conditions of 45% relative humidity and at 24°C. The sound absorption coefficient is given by the ratio of the dissipated power in the studied material to the incident acoustic power [5, 23]. Based on the measured frequency dependencies of the sound absorption coefficient the noise reduction coefficient (NRC) was calculated as the arithmetical average of the sound absorption coefficient at the excitation frequencies 250, 500, 1000 and 2000 Hz [5]. The longitudinal elastic coefficient K_l of the powder bed is similar to Young's modulus of elasticity of the material and was expressed as follows [24, 25]:

$$K_l = c^2\rho_b = \left(4hf_{p1}\right)^2\rho_b \quad (2)$$

where c is the propagating sound speed, ρ_b is the powder bed bulk density, h is the powder bed height and f_{p1} is the primary absorption peak frequency.

4 Results and discussion

As mentioned in the introduction, inorganic nano/micro particles are used as functional fillers in many polymer based composites, where the dominant factors are particle uniformity, shape, diameter and surface chemistry, which influence the physical and material properties of the final product. These properties include for example mechanical strength, fracture performance, thermal behavior, barrier properties, and electrical conductivity [5]. It is very well known from previous studies, that the filler particle-matrix adhesion is of paramount importance for high strength composites preparation. That is why, we have studied surface energy profiles and surface energy distribution by means of iGC testing of the studied materials with respect to obtain their surface wettability characteristics in detail. As shown in Figure 1, observed surface energy profiles have typical exponential decay dependencies, indicating two major areas: the high energy areas observed in the surface coverage regions ranging from 0 to 0.2 depending on the type of the studied powders reaching maximum of the total surface energy in the range from 60 to 85 mJ/m^2 and the low energy areas observed in the surface coverage regions from 0.05 to 1 exhibiting equilibrium total surface energy of about 35 to 60 mJ/m^2. The highest surface reactivity as represented by the observed total surface energy was found for the sample 2 (mica) characteristic with dispersive part of the surface energy dominant over the polar part. The surface energy polar part ranged from 16 to 1 mJ/m^2.

Table 2: Results from the shear cell flow experiments, measured at the consolidation stress of 9 kPa calcium carbonate, mica and perlite (samples 1, 2 and 4) and 22 kPa wollastonite (sample 3) and the temperature of 25°C

Sample	Cohesion [kPa]	UYS [kPa]	MPS [kPa]	FF [-]	AIF [°]	MCS [kPa]
1	0.86	2.98	14.04	4.71	30.13	3.67
2	0.87	3.38	19.50	5.76	35.60	4.25
3	0.77	4.10	64.40	15.70	48.90	8.49
4	0.20	0.78	16.20	20.70	36.50	3.91

UYS – unconfined yield strength, MPS – major principal stress,

FF – flow function, AIF – angle of internal friction, MCS – minor consolidation stress.
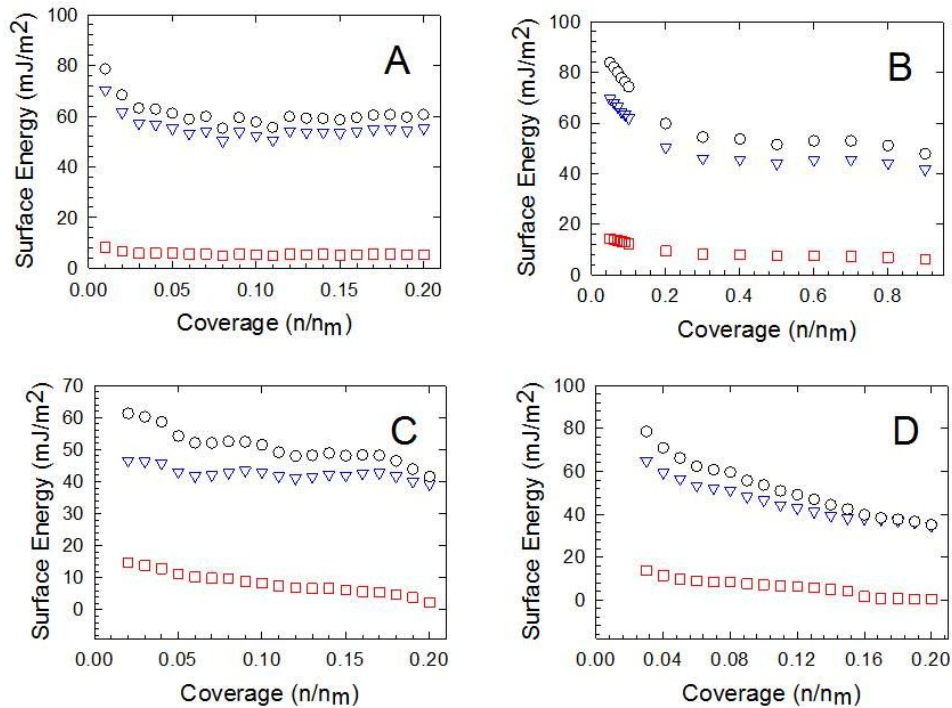
Figure 1: Surface energy profiles of studied fillers: A – calcium carbonate hollow spheres (sample 1), B – mica (sample 2), C – wollastonite (sample 3), D – perlite (sample 4). Square – polar part of the surface energy, triangle – dispersive part and circle – total surface energy

The surface energy distributions of studied powders are shown in Figure 2. These are of a typical peak like shapes where the highest population of 5.2% area increment at the total surface energy of $72 \, \text{mJ/m}^2$ (sample 1) was found. The lowest population of about 0.55% area increment at the total surface energy of $45 \, \text{mJ/m}^2$ was found for the sample 4 (perlite). Similar patterns were observed for the distributions of the polar parts of the surface energy, however, the dominating part was the dispersive energy for all tested powder materials. Obtained dispersive part distributions ranged from 45 to $85 \, \text{mJ/m}^2$ (calcium carbonate, sample 1), from 44 to $84 \, \text{mJ/m}^2$ (mica, sample 2), from 42 to $50 \, \text{mJ/m}^2$ (wollastonite, sample 3) and from 28 to 76 mJ/m^2 (perlite, sample 4). The polar parts distributions ranged from 0 to $17 \, \text{mJ/m}^2$. Density function theory calcu-

lations have theoretically shown that negative surface energies are possible for porous alumina in its high surface area nanocrystalline form [26, 27]. This was attributed to the particularly strongly bound state of dissociated water. However the negative energies for the perlite sample are probably either an artefact of the model or due to its glassy nature.

Results of the powder rheology measurements are shown in Figure 3. These are of a typical yield locus and Mohr's circles dependencies as a function of the applied normal stresses. The obtained individual shear flow parameters are given in Table 2. It is evident, that the most cohesive character of the powder flow was found for the samples 1 (calcium carbonate) and 2 (mica) as indicated by the observed flow functions of 4.7 calcium carbonate (sample
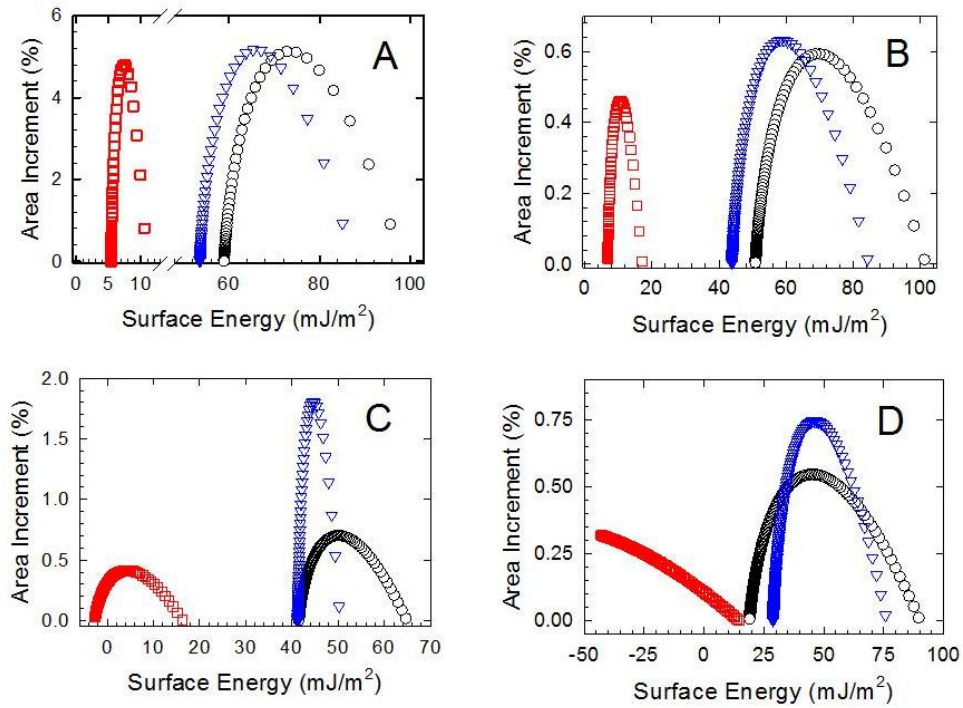
Figure 2: Surface energy distribution of studied fillers: A – calcium carbonate hollow spheres (sample 1), B – mica (sample 2), C – wollastonite (sample 3), D – perlite (sample 4). Square – polar part of the surface energy, triangle – dispersive part and circle – total surface energy
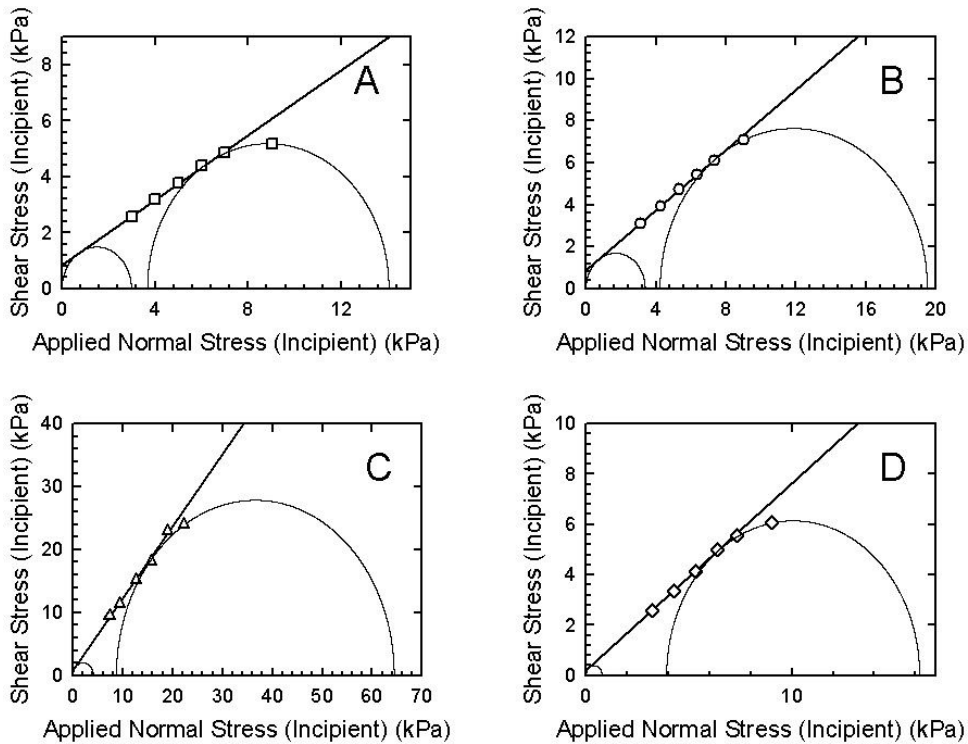

Figure 3: Yield locus and the Mohr's circles of the tested materials as obtained by shear cell experiments at applied 9 kPa consolidation stress (samples 1, 2 and 4) and at 22 kPa consolidation stress (sample 3): A – calcium carbonate hollow spheres (sample 1), B – mica (sample 2), C – wollastonite (sample 3), D – perlite (sample 4)

Table 3: Results of the acoustic and mechanical testing of the studied powder fillers

Sample	Quantity	Material height [mm]				
		10	15	20	50	100
1	NRC [-]	0.149	0.180	0.167	0.167	0.163
	f_{p1} [Hz]	808	544	520	312	304
	c [m·s^{-1}]	32.2	32.6	41.6	62.4	121.6
	K_l [MPa]	2.5	2.6	4.2	9.4	35.5
2	NRC [-]	0.233	0.235	0.222	0.370	0.261
	f_{p1} [Hz]	744	464	344	240	216
	c [m·s^{-1}]	29.8	27.8	27.5	48.0	86.4
	K_l [MPa]	0.4	0.4	0.3	1.0	3.4
3	NRC [-]	0.216	0.191	0.248	0.196	0.216
	f_{p1} [Hz]	736	382	280	168	144
	c [m·s^{-1}]	29.4	22.9	22.4	33.6	57.6
	K_l [MPa]	0.6	0.3	0.3	0.7	2.2
4	NRC [-]	0.106	0.095	0.116	0.136	0.124
	f_{p1} [Hz]	848	600	472	304	296
	c [m·s^{-1}]	33.9	36.0	37.8	60.8	118.4
	K_l [MPa]	1.3	1.4	1.6	4.0	15.3

1) and 5.7 mica (sample 2) typical for cohesive powders. In contrary to this, the observed flow curves for the samples 3 (wollastonite) and 4 (perlite) indicate typical free flow powders behavior, as confirmed also by flow functions exceeding values of 15. The highest magnitude of the major principal stress of 64.4 kPa was found for sample 3 (wollastonite) at a 22 kPa consolidation stress. Other samples exhibited lower values of the major principal stress ranging from 14.04 kPa (sample 1) to 19.5 kPa (sample 2) at 9 kPa consolidation stress. The observed data correspond also with the obtained magnitudes of the unconfined yield strengths of the studied materials, which were ranging from 0.78 kPa (sample 4) to 3.38 kPa (sample 2) at the 9 kPa consolidation stress, and of 4.1 kPa (sample 3) at the 22 kPa consolidation stress.

In general, in the matrix of the sound attenuating material dissipation of the incident acoustic wave is converted to mechanical energy and heat [28]. This proceeds by combination of the following processes. Firstly by friction of the vibrating air molecules on the walls during their penetration into the pores of the sound absorbing material (by lowering kinetic energy of the incident sound field, effectiveness of this process increases with growing porosity of the absorption material). Secondly by decreasing the potential energy of the acoustic wave penetrating into the material (by lowering acoustic pressure due to the heat exchange between air and the skeleton of the absorbing material during periodic pressure changes), and thirdly by non−elastic deformation of the absorbing mate-
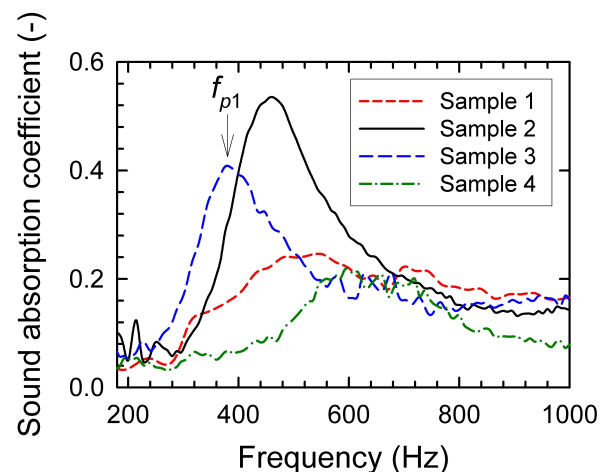
Figure 4: Frequency dependencies of the sound absorption coefficient of studied particular fillers. Powder bed height 15 mm

rial body [29, 30]. Results of sound absorption experiments are shown in Figures 4 and 5 and Table 3.

The highest magnitude of the sound absorption coefficient was 0.54 (at the frequency of 460 Hz) simultaneously with the highest value of the noise reduction coefficient (NRC = 0.235, at the 15 mm powder bed height) were found for the powder bed of the sample 2 (mica) due to its high porosity in comparison to the other tested samples. As mentioned earlier, these results correspond very well with the observed highest cohesion of 0.87 kPa (see Table 2) and the highest surface energy of 72 mJ/m^2 (see Figure 2), as obtained for the sample 2. The lowest poros-
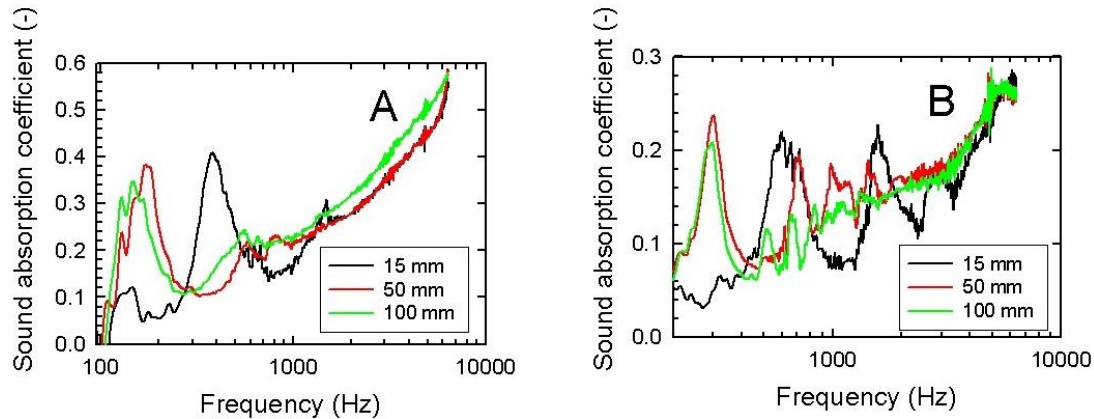
Figure 5: Frequency dependencies of the sound absorption coefficient of studied particular fillers: A – wollastonite (sample 3), B – perlite (sample 4). Inset: Powder bed height in mm
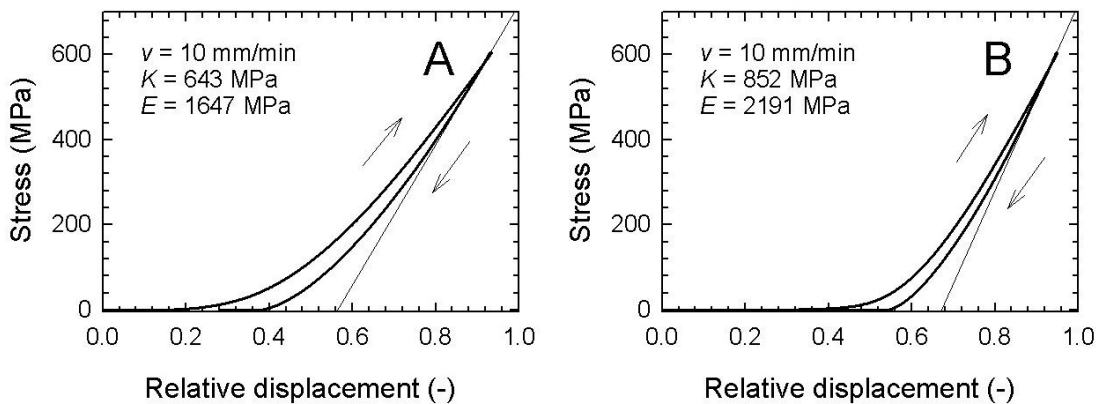

Figure 6: Stress vs relative displacement dependencies observed during chamber uniaxial compression testing (at 10 mm/min deformation rate and 80 kN compression force): A - hollow spheres calcium carbonate filler (sample 1), B - wollastonite filler (sample 3)

ity was found for the sample 4 as indicated both by powder rheology (see the lowest value of the parameter of cohesion of 0.2 kPa in Table 2) and the lowest NRC coefficient of 0.095 at the same bed height as in the case of the mica data. These data correspond very well in the same fashion as in the previous mica (sample 2) with the surface energy distribution, which was the most populated for the perlite (sample 4) at the 45 mJ/m^2, which was found to be the lowest surface energy in comparison with other tested powders.

In Figure 5 results of the effect of the powder bed height on frequency dependencies of the sound absorption coefficient are shown. Here, a typical shift of the primary absorption peak frequency (f_{p1}) position to lower frequencies was found (see Figure 4 and Table 3) with increasing powder bed height [5]. By the application of Eq. (2) the longitudinal elastic modulus (K_l) and propagated sound velocity (c) were calculated. Results indicate, that the highest velocity of the propagated sound wave was found in the calcium carbonate and perlite powders (samples 1 and 4) of 32.6 m/s and 36.0 m/s respectively (for the powder

bed height of 15 mm). These results were confirmed also with the observed highest packing density of the latter calcium carbonate and perlite powders (samples 1 and 4) hence resulting in the obtained highest structural stiffness of the system as reflected in observed values of the K_l being 2.6 MPa calcium carbonate (sample 1) and 1.4 MPa perlite (sample 4).

Results of the uniaxial die compression testing of the calcium carbonate and wollastonite (samples 1 and 3) are shown in Figures 6 and 7. Typical patterns of the loading and unloading curves were obtained with a characteristic hysteresis loop. According to the Eq. (1) the calculated bulk modulus (K) of 643 MPa (calcium carbonate) and 852 MPa (wollastonite) as well as elastic modulus (E) of 1647 MPa (calcium carbonate) and 2191 MPa (wollastonite) were obtained for 10 mm/min deformation rates and 600 MPa maximum compression stress. Results of the effect of the deformation rate on obtained bulk modulus are illustrated for the calcium carbonate (sample 1) in Figure 7. Here a typical increase of the bulk modulus with increasing deforma-
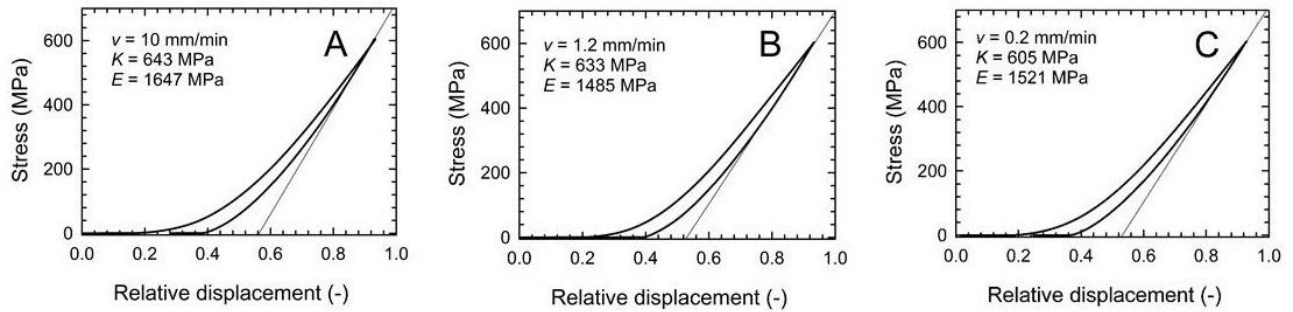
Figure 7: Stress vs relative displacement dependencies observed for hollow spheres calcium carbonate filler (sample 1) during chamber uniaxial compression testing (at 80 kN compression force): A - 10 mm/min deformation rate, B - 1.2 mm/min deformation rate and C. - 0.2 mm/min deformation rate
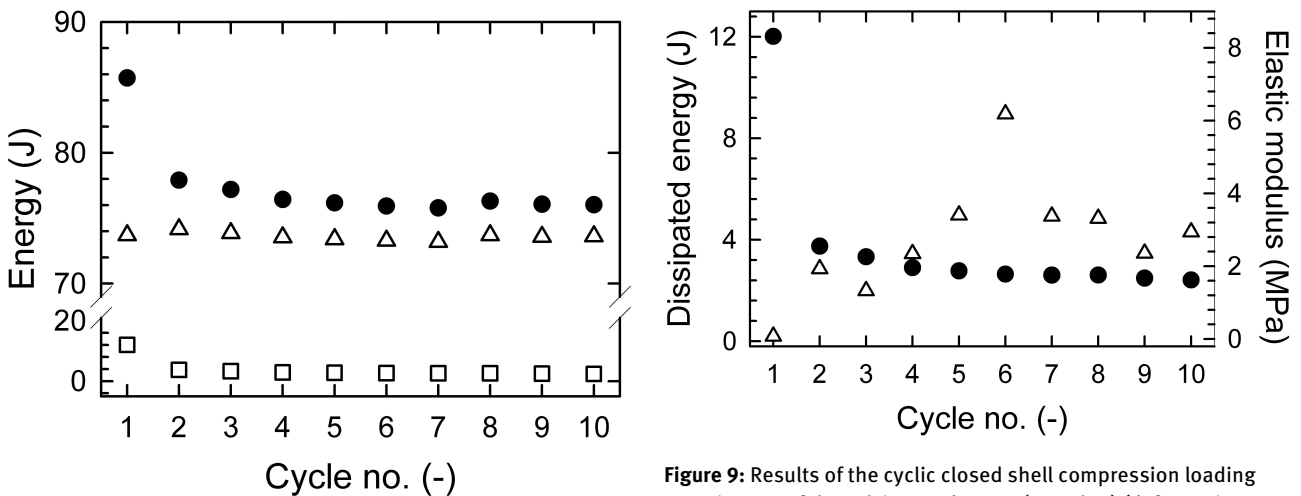

Figure 8: Results of the cyclic closed shell compression loading experiments of the calcium carbonate (sample 1) (deformation rate 10 mm/min, maximum force 80 kN): full circle – input energy (J), triangle up – stored energy (J), square – dissipated energy (J)

Figure 9: Results of the cyclic closed shell compression loading experiments of the calcium carbonate (sample 1) (deformation rate 10 mm/min, maximum force 80 kN): full circle – dissipated energy (J), triangle up – elastic modulus (MPa)

tion rate was found from 605 MPa for deformation rate of 0.2 mm/min to 643 MPa for 10 mm/min deformation rate. Similar results were also found for all other tested samples. Results of the cyclic die compression loading experiments for calcium carbonate (sample 1) are shown in Figures 8 and 9. In these experiments the interest was to follow the progressing elastic-plastic deformation followed by the breakage of the hollow spheres of the calcium carbonate hollow spheres. There were followed the input energy, stored energy as well as dissipated energy during individual deformation cycles. It was found, that with an increasing number of cycles a stiffer internal structure of the compressed material was created, as indicated by increased stored energy in the second and third cycles due to the proceeding elasto-plastic contact deformation process and decreasing dissipated energy from 12 J (cycle 1) to 3.5 J (cycle 3) reaching up the linearly decreasing equi-
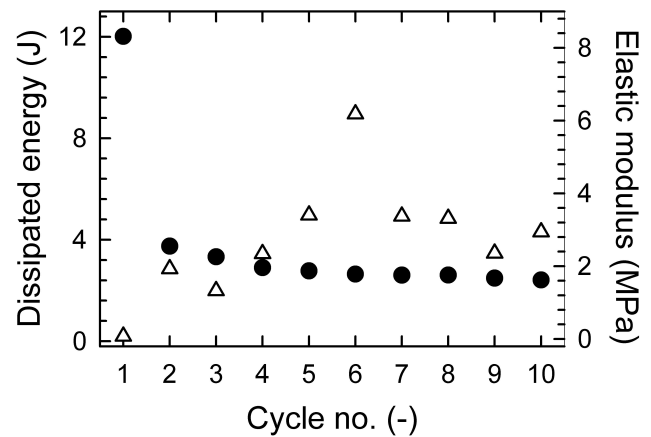
librium energy dissipation of 2.8 J (cycle 10). The complexity of the observed sequence of the individual deformation events proceeding in the course of the die compression of the tested hollow sphere calcium carbonate (sample 1) is evident from the Figure 9 (elastic modulus vs. cycle no. dependency). At the beginning of the compression process a clear increase in the elastic modulus between cycles 1 and 2 indicates progressing feed of loose packing followed by elastic-plastic contact deformation as found by Berg *et al.* [20]. The latter step was followed by an observed decrease of the elastic modulus from 1.93 MPa (cycle 2) to 1.33 MPa (cycle 3) due to the progressive pore filling by fine particles followed by plastic deformation of particles to create large contact areas as indicated by a linear increase of the *E* in the consecutive cycles from cycle 3 to cycle 6, reaching a maximum value of elastic modulus 6.18 MPa. This reflects the state of the compressed matrix still preserving the hollow spherical structure of the filler material. This stage was then followed by proceed-

ing breakage of the individual hollow spheres, edges and particle breakage, pore filling as indicated by preserving constant magnitude of the E between cycle no. 7 and 8 followed by its decrease to 2.36 MPa (cycle 9) and its recovery to 2.94 MPa during cycle 10. This complex pattern indicates the final plastic deformation process progressing in the material as earlier confirmed by our creep experiments with high density poly(ethylene)/calcium carbonate hollow spheres composites, where there was clear evidence of the higher plasticity behavior for composite HDPE/CaCO$_3$ hollow spheres material compared to the virgin HDPE matrix [31].

5 Conclusions

It was found in this study, that the particle surface energy and the particle shape strongly affect the packing density of the powder bed of the tested filler materials as characterized by acoustic and mechanical material testing. These were performed by measurement of the frequency dependence of the sound absorption coefficient, which was found to be higher in the case of the higher porosity and thus lower bulk density powder materials. This affects the powder materials bulk mechanical properties in such a manner that in the case of their application as a filler material in complex composite systems it is strongly affecting their final plastic-elastic mechanical behavior. Surface energy profiles and surface energy distributions determined by surface energy analysis by means of iGC technique showed its robustness for in detail characterization of the wetting characteristics of the studied powder filler materials. These data showed clear convergence with the powder rheological measurements, where the characteristics of the powder flow at defined consolidation stresses were mirroring either the high cohesion powders properties connected with the high surface energy or powder free flowing characteristics, as reflected in low cohesion of the powder matrix. Due to the prospective application of these mineral materials in composites engineering applications, the hollow sphere calcium carbonate micro/nano filler material was tested for its mechanical behavior response on uniaxial die compression tests. These experiments were done earlier by other authors for the same particulate planar filler materials [14], who found a complex compression mechanism. This high complexity of the latter deformation processes was confirmed also in this study, where the sequence of the consecutive particle packing, particle elastic-plastic deformation, pore filling, plastic deformation and breakage of particles, edges and final plastic deformation

of the entire compressed body were clearly identified from the cyclic stress vs. relative displacement measurements.

References

[1] Sherwood J.A., Dignam L.J.J., Dobbins T., Boeman R.G., U.S. Composites Manufacturing Industry Technical Roadmap, Facilitating Industry by Engineering, Roadmapping and Science (FIBERS) to Advance U. S. Manufacturing of Composites, 2017, 1-53.

[2] Anwar A., Kanwal Q., Akbar S., Munawar A., Durrani A., Farooq M.H., Synthesis and characterization of pure and nanosized hydroxyapatite bioceramics, Nanotechnol. Rev., 2017, 6, 149-157.

[3] Mahna S., Singh H., Tomar S., Bhagat D., Patnaik A., Kumar S.R., Dynamic mechanical behavior of nano-ZnO reinforced dental composite, Nanotechnol. Rev., 2019, 8, 90-99.

[4] Power A.C., Gorey B., Chandra S., Chapman J., Carbon nanomaterials and their application to electrochemical sensors: a review, Nanotechnol. Rev., 2018, 7, 19-41.

[5] Lapčík L., Vašina M., Lapčíková B., Otyepková E., Waters K.E., Investigation of advanced mica powder nanocomposite filler materials: Surface energy analysis, powder rheology and sound absorption performance, Compos. Pt. B-Eng., 2015, 77, 304-310.

[6] Ottani S., Valenza A., Lamantia F.P., Shear characterization of CaCO$_3$-filled linear low-density polyethylene, Rheol. Acta, 1988, 27, 172-178.

[7] Zhu B.L., Wang J., Zheng H., Ma J., Wu J., Wu R., Investigation of thermal conductivity and dielectric properties of LDPE-matrix composites filled with hybrid filler of hollow glass microspheres and nitride particles, Compos. Part B-Eng., 2015, 69, 496-506.

[8] Lapčík L., Ruszala M.J.A., Vašina M., Lapčíková B., Vlček J., Rowson N.A., Grover L.M., Greenwood R.W., Hollow spheres as nanocomposite fillers for aerospace and automotive composite materials applications, Compos. Pt. B-Eng., 2016, 106, 74-80.

[9] Kauffman S.H., Leidner J., Woodhams R.T., Xanthos M., Preparation and classification of high aspect ratio mica flakes for use in polymer reinforcement, Powder Technol., 1974, 9, 125-133.

[10] Michalowski M., Simulation model for frictional contact of two elastic surfaces in micro/nanoscale and its validation, Nanotechnol. Rev., 2018, 7, 355-363.

[11] Song J.H., Evans J.R.G., A die pressing test for the estimation of agglomerate strength, J. Am. Ceram. Soc., 1994, 77, 806-814.

[12] Gai G.S., Yang Y.F., Fan S.M., Cai Z.F., Preparation and properties of composite mineral powders, Powder Technol., 2005, 153, 153-158.

[13] Koehler J.M., Visaveliya N., Knauer A., Controlling formation and assembling of nanoparticles by control of electrical charging, polarization, and electrochemical potential, Nanotechnol. Rev., 2014, 3, 553-568.

[14] Stasiak M., Tomas J., Molenda M., Rusinek R., Mueller P., Uniaxial compaction behaviour and elasticity of cohesive powders, Powder Technol., 2010, 203, 482-488.

[15] Kenny W.J., Piret E.L., Slow Compression Crushing of Single Particles of Glass, AIChE J., 1961, 7, 199-202.

[16] Nysaeter T.O., Enstad G.G., On the elastic modulus of powders, Part. Part. Syst. Charact., 2012, 29, 53-63.

[17] Wu C., Ruddy O., Bentham A., Hancock B., Best S., Elliott J., Modelling the mechanical behaviour of pharmaceutical powders during compaction, Powder Technol., 2005, 152, 107-117.

[18] Lapčík L., Otyepka M., Otyepková E., Lapčíková B., Gabriel R., Gavenda A., Prudilová B., Surface heterogeneity: Information from inverse gas chromatography and application to model pharmaceutical substances, Curr. Opin. Colloid Interface Sci., 2016, 24, 64-71.

[19] Mohammadi-Jam S., Waters K.E., Inverse gas chromatography applications: A review, Adv. Colloid Interface Sci., 2014, 212, 21-44.

[20] Berg S., Jonsen P., Haggblad H., Experimental characterisation of $CaCO_3$ powder mix for high-pressure compaction modelling, Powder Technol., 2010, 203, 198-205.

[21] Fossum A.F., Senseny P.E., Pfeifle T.W., Mellegard K.D., Experimental-determination of probability-distributions for parameters of a Salem Limestone cap-plasticity-model, Mech. Mater., 1995, 21, 119-137.

[22] International Organization for Standardization, Acoustics-Determination of sound absorption coefficient and impedance in impedance tubes-Part 2: Transfer-function method, ISO 10534-2, 1998,.

[23] Sgard F., Castel F., Atalla N., Use of a hybrid adaptive finite element/modal approach to assess the sound absorption of porous materials with meso-heterogeneities, Appl. Acoust., 2011, 72, 157-168.

[24] Okudaira Y., Kurihara Y., Ando H., Satoh M., Miyanami K., Sound-absorption measurements for evaluating dynamic physical-properties of a powder bed, Powder Technol., 1993, 77, 39-48.

[25] Allameh-Haery H., Kisi E., Pineda J., Suwal L.P., Fiedler T., Elastic properties of green expanded perlite particle compacts, Powder Technol., 2017, 310, 329-342.

[26] Lodziana Z., Topsoe N.Y., Norskov J.K., A negative surface energy for alumina, Nature Materials, 2004, 3, 289-293.

[27] Lodziana Z., Topsoe N.Y., Norskov J.K., Negative surface energy - Clearing up confusion - Response, Nature Materials, 2005, 4, 186-186.

[28] Leena M., Srinivasan S., Prabhaharan M., Evaluation of acoustical parameters and thermal conductivity of TiO2-ethylene glycol nanofluid using ultrasonic velocity measurements, Nanotechnol. Rev., 2015, 4, 449-456.

[29] Lapčík L., Joch M., Vašina M., Lapčíková B., Fojtů D., Juricka M., Sound and vibration damping materials for aeronautics application, EURONOISE 2012, 2012, 826-828.

[30] Lapčík L., Cetkovský V., Lapčíková B., Vašut S., Materials for noise and vibration attenuation, Chem. Listy, 2000, 94, 117-122.

[31] Lapčík L., Maňas D., Vašina M., Lapčíková B., Řezníček M., Zádrapa P., High density poly(ethylene)/CaCO3 hollow spheres composites for technical applications, Compos. Pt. B-Eng., 2017, 113, 218-224.